A sol-gel based silver nanoparticle/polytetrafluorethylene (AgNP/PTFE) coating with enhanced antibacterial and anti-corrosive properties

Zhang, Shuai; Liang, Xinjin; Gadd , Geoffrey Michael ; Zhao, Qi

Published in:
Applied Surface Science

DOI:
10.1016/j.apsusc.2020.147675

Publication date:
2021

Document Version
Publisher's PDF, also known as Version of record

Applied Surface Science 535 (2021) 147675

Contents lists available at ScienceDirect

Applied Surface Science

journal homepage: www.elsevier.com/locate/apsusc

A sol–gel based silver nanoparticle/polytetrafluorethylene (AgNP/PTFE) coating with enhanced antibacterial and anti-corrosive properties

Shuai Zhang[a,d], Xinjin Liang[b,c], Geoffrey Michael Gadd[c], Qi Zhao[d,*]

[a] School of Mechanical and Aerospace Engineering, Queen's University Belfast, Belfast BT9 5AG, UK
[b] School of Chemistry and Chemical Engineering, Queen's University Belfast, Belfast BT9 5AG, UK
[c] School of Life Sciences, University of Dundee, Dundee DD1 5EH, UK
[d] School of Science and Engineering, University of Dundee, Dundee DD1 4HN, UK

ARTICLE INFO

Keywords:
Silver
Polytetrafluoroethylene
Biofilm
Antibacterial activity
Corrosion

ABSTRACT

In this research, a silver nanoparticle/polytetrafluorethylene (AgNP/PTFE) coating for metallic implants was fabricated using a facile layer-by-layer coating method. PTFE nanoparticles were immobilized in a sol–gel matrix and dip-coated onto 316L stainless steel *via* a mussel-inspired approach followed by AgNP deposition. Benefiting from the synergistic effect of antibacterial AgNP and non-stick PTFE, the AgNP/PTFE coating exhibited superior antibiofilm activity against *Escherichia coli* WT F1693 and enhanced corrosion resistance. Compared with surfaces only coated with PTFE, the AgNP/PTFE coated surfaces were capable of sustained release of silver ions, inhibiting up to ~50% bacterial biomass accumulation after 7 days. To understand the anti-adhesion mechanism, both classic DLVO and XDLVO theories were used to model and explain bacterial adhesion. Despite concerns that an over-release of silver ions may cause toxic effects towards mammalian cells, the coating procedures offered ease of control over the silver loading, making it potentially useful for preventing metallic implant-associated infections.

1. Introduction

To date, bacterial infection remains a critical challenge for metallic implants [1,2]. As a basic survival strategy, bacteria predominantly live as sessile cells on surfaces rather than as planktonic cells in suspension, and implant surfaces provide particularly attractive sites for bacterial adhesion and subsequent biofilm formation [3,4]. For this reason, numerous strategies have been developed to endow implant surfaces with antibacterial properties to prevent/retard bacterial contamination [5–10]. Silver (Ag)-based coatings have aroused intense interest as silver has broad-spectrum antibacterial activity and a low risk of developing bacterial resistance [11–15]. However, implants coated with silver alone have only demonstrated limited success in clinical studies [16–18]. Despite concerns that silver release may cause toxicity in humans, insufficient silver ion (Ag^+) release has nonetheless been considered as the main reason for the failure of silver-coated implants. To solve this problem, silver nanoparticles (AgNPs) have been strategically used to replace bulk silver in coatings to improve antibacterial efficiency with considerable success [19–22]. Owing to the large specific surface area, AgNP demonstrated enhanced antibacterial activity allowing a rapid release of Ag^+ which affected membrane permeability and DNA replication, leading to cytoplasm leakage and even cell death [23,24].

Anti-adhesive coatings are another potential solution to overcome these challenges. Although bacterial adhesion is a complex process, the first adhesion phase is believed to be governed by physical and/or chemical interactions between the planktonic cells and the surface [25]. For example, low-energy surfaces are considered to be less sensitive to bacterial adhesion because of weaker bonding at the interface [26]. Polytetrafluoroethylene (PTFE) is one of the most biocompatible medical materials and has long been known for its non-stick properties [27]. These properties are believed to result from the extremely strong cohesive forces of the PTFE molecules that minimize van der Waals interactions between the surface and bacterial cells [28]. To date, numerous studies have reported success in reducing bacterial adhesion by incorporating PTFE nanoparticles into the coating matrix [29–32]. Moreover, due to the extremely low coefficient of friction, PTFE has also been applied to implantable devices for the provision of enhanced lubricity to minimize patient discomfort [33]. However, the conventional fabrication process often requires specific equipment and may introduce toxic substances into the coatings.

Recently, sol–gel techniques have emerged as an effective method

* Corresponding author.
E-mail address: q.zhao@dundee.ac.uk (Q. Zhao).

https://doi.org/10.1016/j.apsusc.2020.147675
Received 8 July 2020; Received in revised form 21 August 2020; Accepted 24 August 2020
Available online 29 August 2020

for synthesizing nanocomposite coatings by entrapment of functional substances into the sol–gel matrix [34]. During the sol–gel process, the substances are mixed with hydrolyzed sol and gradually trapped in the network structure in a capsule- or cage-like manner [35]. This simple feature makes it possible to immobilize PTFE within the coating matrix to provide an anti-adhesive, corrosion-resistant and lubricant surface for implants. Moreover, the sol–gel matrix serves as a platform that allows further modification. Roe et al. [36] previously described a cost-effective AgNP coating technology, that could be applied to nearly any type of substrate material, which demonstrated excellent potential for reducing the risk of infection. Therefore, it would be ideal to combine antibacterial AgNP with a non-stick PTFE coating to provide enhanced resistance of the implant surface to bacterial contamination.

In this research, we fabricated an AgNP/PTFE (AP) coating for metallic implants *via* a facile mussel-inspired approach. PTFE nanoparticles were incorporated into a sol–gel matrix and coated onto polydopamine (PDA) functionalized substrates using a dip-coating technique followed by AgNP deposition. Antibacterial and antibiofilm activities were evaluated using *Escherichia coli* WT F1693. Corrosion resistance was assessed by potentiodynamic polarization measurements, and cytotoxicity was evaluated using the 3-(4,5-dimethylthiazol-2-yl)-2,5-diphenyltetrazolium bromide (MTT) assay method with mouse fibroblast cells L929.

2. Experimental

2.1. Preparation of AgNP/PTFE (AP) coatings

Commercially available 316L stainless steel (316L SS) plates (size 10 mm × 10 mm × 1 mm) were used as substrates and electropolished before further treatment. First, the plates were immersed in a dopamine solution (2 mg/mL dopamine in 10 mM Tris-HCl buffer, pH = 8.5) (Sigma-Aldrich, UK) for 24 h to allow the deposition of a polydopamine (PDA) sublayer. A titanium (IV) butoxide (TBOT) (Sigma-Aldrich, Dorset, UK) sol - PTFE mixture (PTFE particles: 2.0 g/L, particle size of 200–300 nm, Polysciences, Inc., USA) was prepared and hydrolyzed at room temperature *via* an acid catalyzed sol–gel process. The volume ratios for TBOT:EtOH:0.1 M HNO_3 were 1:40:3 and the mixture was mechanically stirred for 24 h. The PDA-coated plates were vertically dipped into the mixture and withdrawn at a constant speed of 5 mm/s. To ensure coating uniformity, the coating process was repeated 3 times and air dried at room temperature for at least 20 min. The plates were then immersed into an aqueous solution containing 5 mL/L Tween 20 (Sigma-Aldrich, Dorset, UK), 0.85 g/L sodium saccharine (Sigma-Aldrich, Dorset, UK), 0.45 g/L silver nitrate (Sigma-Aldrich, Dorset, UK) and 3.5 mL/L N, N, N', N' - tetramethylethylenediamine (Sigma-Aldrich, Dorset, UK) at 60 °C for 1–12 h to allow AgNP deposition. After being removed from solution, the plates were subsequently rinsed with 0.1 M HNO_3, deionized water and ethanol, air dried and stored in darkness before further testing.

2.2. Surface characterization

The surface morphology of the coatings was characterized using a field emission-scanning electron microscope (FE-SEM, JEOL JSM-7400F, Tokyo, Japan) and atomic force microscope (AFM, Dimension 3000, Santa Barbara, CA, USA). Surface chemistry composition was analyzed by using energy-dispersive X-ray spectrometry (EDX, QX200, Bruker, USA). The distribution of PTFE and Ag particles was monitored by EDX elemental mapping across the entire surface of the coatings. ImageJ (LOCI, University of Wisconsin, Wisconsin, USA) was used to identify and calculate the particle size distributions of PTFE and AgNP from random SEM images. The surface free energy of the coatings was calculated using the van Oss approach [26,29] and contact angles were measured using a Dataphysics OCA-20 contact angle analyzer (DataPhysics Instruments GmbH, Filderstadt, Germany).

2.3. Silver loading and release

The effect of deposition time on silver loading at the surface was characterized. The AP coated plates (n = 3) with deposition time ranging from 1 to 12 h were separately immersed in 30% HNO_3 for at least 10 h to ensure complete dissolution of the Ag. The Ag concentration was then determined by using atomic absorption spectrophotometry (Perkin Elmer, AAnalyst 400, USA). To characterize silver release from the AP coatings, the AP coated plates (n = 3) were separately immersed in 3 mL of PBS at 37 °C for up to 7 days. The PBS solution was collected and refreshed every day and the silver concentration was measured by using AAS. Silver loading and release were expressed in $\mu g/cm^2$.

2.4. Antibacterial activity test

Escherichia coli WT F1693 was obtained from the Institute of Infection and Immunity, Nottingham University, UK. *E. coli* WT F1693 was inoculated onto tryptone soya agar (TSA) plates and cultured at 37 °C overnight before sub-culturing in Tryptic Soy Broth (TSB). The bacteria were harvested at the mid-exponential phase and diluted with nutrient media (10% TSB in PBS) to approximately 10^6 CFU/mL. To determine antibacterial activity, the samples (n = 6) were co-incubated with 3 mL of the diluted bacterial suspension at 37 °C for 7 days. The optical density, at 600 nm, of the bacterial suspension was measured daily. To avoid any accumulative effects of Ag^+, the bacterial suspension was refreshed every day. The reduction of bacterial growth was calculated using the following equation:

$$\text{Reduction percentage} = (C_{OD} - E_{OD})/C_{OD} \times 100\%$$

where C_{OD} and E_{OD} are the OD_{600} values of the control wells containing only bacteria and the wells containing both samples and bacteria, respectively.

2.5. Live/dead biofilm staining

After 1 or 7 days of incubation, the samples were removed from the bacterial suspension and air dried after being carefully washed with PBS. The samples were then stained in the dark using the LIVE/DEAD Baclight bacterial viability kit L13152 (Fisher Scientific, UK) for 15 min. A fluorescence microscope (OLYMPUS BX 41, Tokyo, Japan) was used to observe adhered cells and their viability was determined using Image Pro Plus software (Media Cybernetics, Rockville, USA). Living bacterial cells were stained fluorescent green while dead cells were stained fluorescent red. Biomass on the 316L SS, PTFE and AP coated surfaces was assessed using Gram's crystal violet staining assay [37].

2.6. Corrosion test

The anticorrosion performance of the coatings was investigated using a potentiodynamic polarization test using a CorrTest Electrochemistry Workstation in PBS at room temperature. Measurements were conducted in a conventional three-electrode cell consisting of a platinum (Pt) counter electrode, a saturated calomel electrode (SCE) as the reference electrode, and the sample (exposed area: 1 cm^2) as the working electrode. Prior to electrochemical measurements, all the samples were immersed in PBS for 1 h to achieve stable Open Circuit Potentials (OCP, E_{oc}). The Corrosion Potential (E_{corr}) and Corrosion Current Density (I_{corr}) were obtained by the Tafel extrapolation method from the potentiodynamic polarization curves at a scan rate of 5 mV/s.

2.7. Cytotoxicity assays

The cytotoxicity of the coatings was assessed *in vitro* by an MTT

assay using mammalian mouse fibroblast cells L929 according to our previous studies [13,19]. The L929 cells were continuously grown in Eagle's minimum essential medium (MEM) supplemented with fetal bovine serum (10%), penicillin (100 mg/mL) and streptomycin (100 mg/mL) until achieving confluence. Subsequently, the cells were collected and seeded in 24 well plates at ~10^5 cells/well and incubated with the samples (n = 4) for up to 72 h. The relative cell viability (%) was determined by comparing the absorbance at 570 nm with the control wells which contained only cells. Cell morphology was examined using both optical microscopy (Leica DFC3000, Leica, Wetzlar, Germany) and confocal microscopy (Leica SP8 confocal microscope, Wetzlar, Germany).

2.8. Statistical analysis

All data were analyzed using one-way ANOVA and represented as means ± standard deviation. $p < 0.05$ was considered significant and $p < 0.01$ was considered highly significant.

3. Results and discussion

3.1. Surface characterization

The AP coating process is demonstrated in Scheme 1. According to our previous study [38], the mussel-inspired PDA sublayer could significantly increase the surface wettability of stainless steel and enable it to resist coating rupture and crack propagation. Upon oxidation, dopamine was transformed to 5,6-dihydroxyindole (DHI) through intermolecular cyclization in a weak alkaline solution and finally self-polymerized to PDA that deposited on the 316L SS surface [39–43]. Subsequently, the TBOT precursor sol was thoroughly mixed with the PTFE nanoparticles followed by a dip-coating process. Previous studies demonstrated that catechol groups in PDA can effectively chelate with Ti(IV) and this strong interaction would promote complete and tight contact between the sol–gel matrix layer and substrate [44,45]. Finally, the AP coating was obtained by continuous AgNP deposition. As seen in Fig. 1a and d, PTFE particles with an average diameter of 509.0 ± 12.1 nm aggregated and were entrapped in the coating matrix. Despite attempts having been made to use surfactants (particularly fluorosurfactants) to improve dispersion of PTFE in coatings and tested with variable success [46–48], our results showed that surfactants damaged the coating integrity by creating multiple holes after solvent evaporation (data not shown). The AgNPs were uniformly deposited on the coating matrix and the size distribution was relatively narrow (~5–30 nm) considering the simplicity of the deposition process. EDX analysis showed the typical surface composition and demonstrated the presence of F and Ag (Fig. 1b), with the EDX mapping results further indicating homogenous distributions of PTFE and AgNP in the coating matrix (Fig. 1c). The Cr and Fe characteristic peaks (Fig. 1b) were from the 316L SS substrate. To investigate the influence of AgNP deposition on surface morphology, the deposition time was controlled from 1 h to 12 h. Water contact angle analysis showed that surface hydrophobicity was slightly increased with the deposition time (Fig. 1e). This could be attributed to the fact that continuous AgNP deposition increases surface roughness and causes a net increase in surface energy during wetting, making the hydrophobic surface more hydrophobic [49]. To verify this, the surface roughness of the AP coatings was determined by AFM. As demonstrated in Fig. 1f, the surface roughness increased from 134.7 ± 3.9 nm (PTFE coating) to 158.1 ± 2.7 nm (AP-1, deposition time of 6 h) and 177.3 ± 5.1 nm (AP-2, deposition time of 12 h), respectively. In comparison, the uncoated 316L SS substrate showed a smoother surface (59.4 ± 6.1 nm).

3.2. Antibacterial activity and biofilm adhesion

For silver-based coatings, their antibacterial activity is directly proportional to the concentration of released silver ions [50]. In this study, the relationship between deposition time and silver loading at the surface was characterized. As seen in Fig. S1, the silver concentrations deposited at the surface gradually increased with deposition time reaching 24.8 ± 2.7 μg/cm^2 and 68.7 ± 3.4 μg/cm^2 after 6 h and 12 h of deposition, respectively. The silver deposition was relatively slow in the first 2 h (~2.4 μg/cm^2·h) and gradually accelerated to a constant rate of ~ 7.2 μg/cm^2·h after 6 h. The low initial deposition rate could be ascribed to the slow nucleation process that led to insufficient silver nanoparticle formation in the vicinity of the surface. Owing to the presence of saccharinate anions, the resulted silver precursor (silver saccharinate) was reduced to stable silver nanoparticles predominantly monodisperse in size that could firmly attach to the surfaces [51]. With the coating time from 2 h to 6 h, the concentration of silver nanoparticles gradually increased, which consequently accelerated silver deposition until a balance was achieved (i.e. the rate of

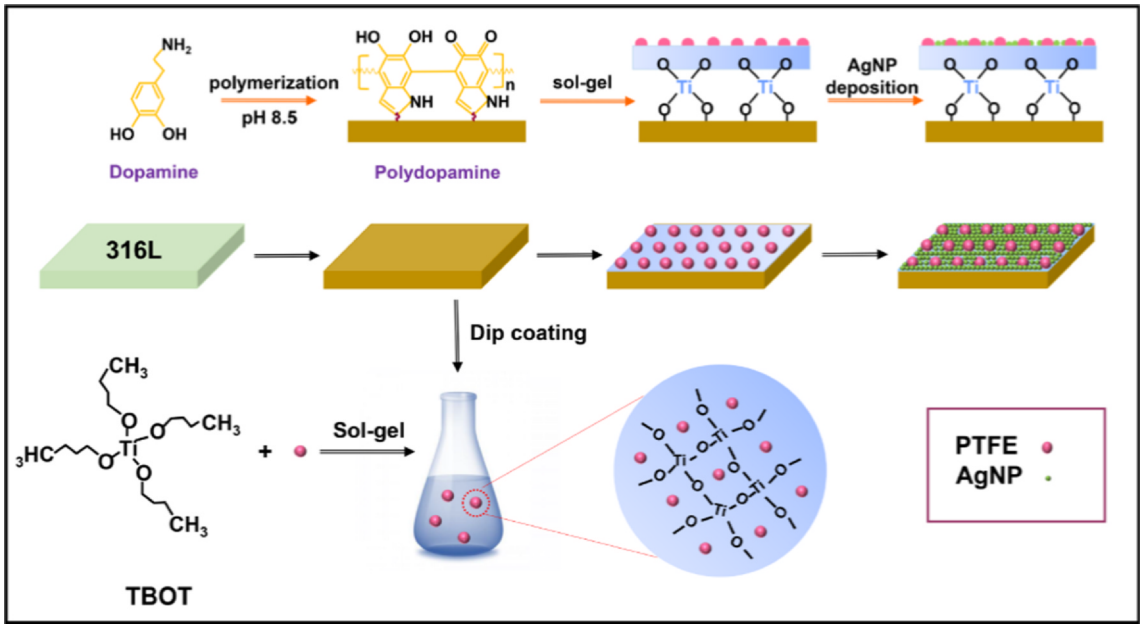

Scheme 1. Diagram of the AP coating process.

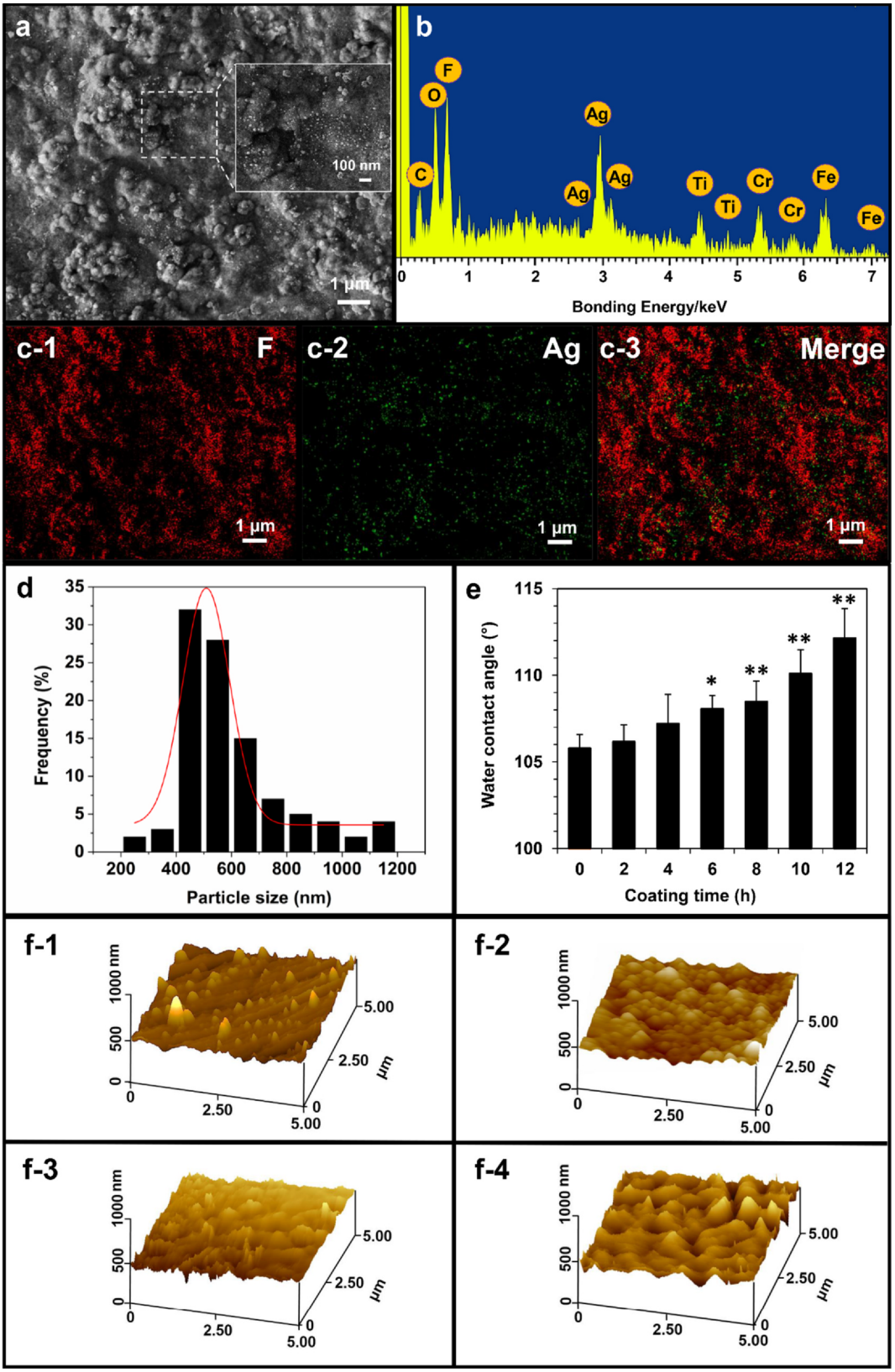

Fig. 1. (a) Typical SEM image of the AP coatings; (b) Semi-quantitative results of EDX; (c) EDX mappings of SEM image a; (d) Size distribution of the PTFE particles and Gaussian fitting; (e) Water contact angle as a function of AgNP deposition time; (f) Typical AFM images of 316L SS (f-1), PTFE (f-2), AP-1 (f-3) and AP-2 (f-4). Bars represent standard deviation of the mean (n = 6). (AP-1 represents the AP coating after 6 h deposition, AP-2 represents the AP coating after 12 h deposition) (*$p < 0.05$, **$p < 0.01$ compared with PTFE coating).

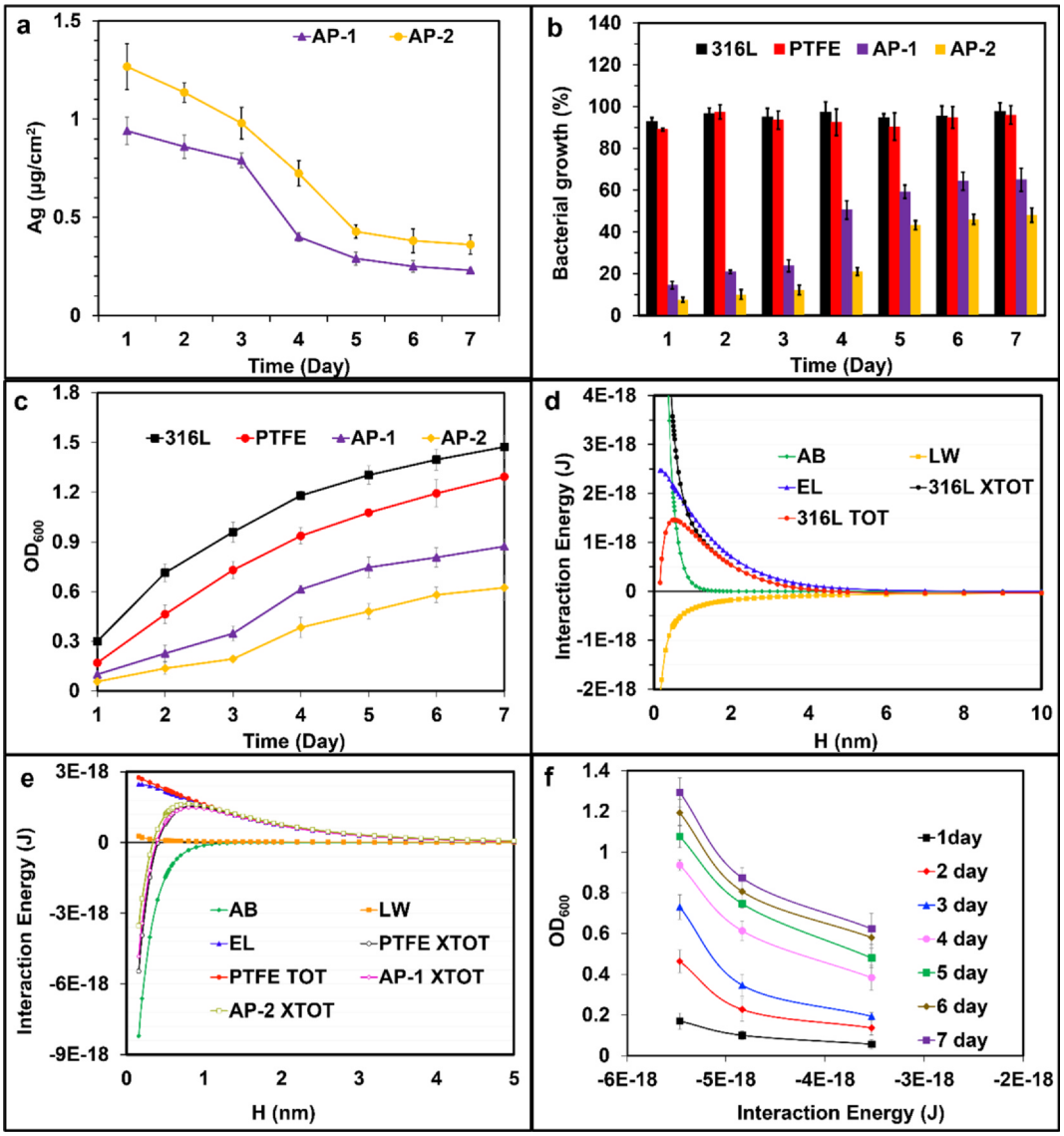

Fig. 2. (a) Ag^+ release profiles from the AP coated samples over time; (b) Bacterial growth in the presence of different samples; (c) Biomass formation on different sample surfaces over time; Effects of separation distance (H) on interaction energy for (d) 316L SS and (e) AP coated surfaces; (f) Effects of the minimum total interaction energies on *E. coli* WT F1693 adhesion at 0.157 nm over time. Bars represent standard deviation of the mean.

silver nanoparticle formation = the rate of silver deposition). Fig. 2a shows Ag^+ release curves from two AP coatings with different deposition times over time. Ag^+ release followed a similar trend in both groups, i.e. a burst release in the initial phase (first 3 days) and a more gradual release in the second phase. Molleman et al. [52] demonstrated that the burst Ag^+ release was attributable to a fast oxidative dissolution process, after which a new stable surface state was built with subvalent silver, yielding a slower but sustained Ag^+ release. Over the first 3 days, the total amounts of silver released from AP-1 (6 h) and AP-2 (12 h) were 2.59 ± 0.17 μg/cm^2 and 3.38 ± 0.25 μg/cm^2, respectively. In comparison, the Ag amounts in the last 3 days were 0.77 ± 0.07 μg/cm^2 and 1.17 ± 0.14 μg/cm^2, respectively. The total amount of silver released from AP-2 (7.7% of coated silver) in 7 days was ~40% higher than that from AP-1 (15.2% of coated silver).

To assess the long-term antibacterial activity of the AP coatings, samples were co-incubated with *E. coli* in a nutrient-rich culture medium for up to 7 days and the cell density of each culture was monitored and compared with the control group. As shown in Fig. 2b, the AP-1 and AP-2 coated samples significantly inhibited *E. coli* growth over the test period when compared with uncoated 316L SS and PTFE coated samples. For both AP-1 and AP-2, growth inhibition was more noticeable in the first 3 days as the coatings were able to release a relatively large amount of Ag^+ to inhibit bacterial growth. The results showed that AP-1 and AP-2 could inhibit by ~75% and ~90% bacterial growth over the initial 3 days, respectively. After 7 days, AP-1 and AP-2 still exhibited significant antibacterial activity, reducing by ~40% and ~50% of bacterial growth, respectively. In comparison, uncoated 316L SS and PTFE coated samples demonstrated no significant ($p > 0.05$) reduction in bacterial growth over the test period.

The anti-adhesion efficacy of the AP coatings was assessed by live/dead staining and the total biofilm biomass was quantitatively determined by crystal violet staining. In general, the amount of cumulative biomass increased with incubation time for all the surfaces (Fig. 2c). The AP-2 exhibited the best anti-adhesive efficacy, reducing by ~60% and ~50% of biomass accumulation when compared with 316L SS and PTFE coating after 7 days' culturing, respectively. The PTFE coating only demonstrated short-term anti-adhesive activity, reducing by ~45% biomass adhesion on the first day as compared with 316L SS, while AP-1 and AP-2 inhibited by ~65% and ~80% of biomass formation. As seen in Fig. 3, after 1 day's culture, apparent bacterial

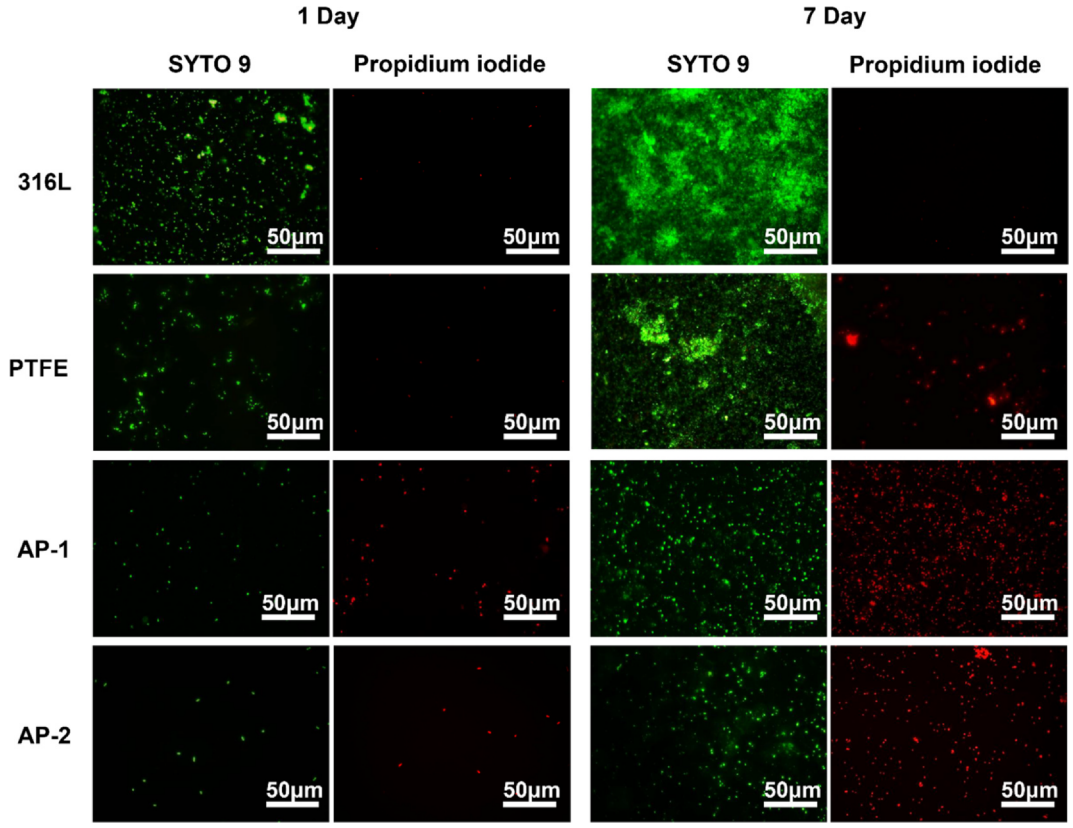

Fig. 3. Live/dead assay: fluorescence microscope images of *E. coli* on the 316L, PTFE, AP-1 and AP-2 after 1 day and 7 day's co-culture. Typical images are shown from one of several examinations.

aggregation was observed on the 316L SS surface although a mature biofilm was not formed. In comparison, only dispersed bacterial cells were found on the PTFE, AP-1 and AP-2 coatings. After 7 days, the mature *E. coli* biofilm had established and aggregated on the 316L SS surface, but dead cells were hardly detected. Large biofilm clusters accumulated on the PTFE coatings, but only a slight aggregation of *E. coli* was observed on the AP-1 and AP-2 coatings. Moreover, a large number of dead cells were found on the AP coatings which could be ascribed to the bactericidal Ag^+ released from the coatings.

3.3. Effect of interaction energy on biofilm adhesion

Over the last few decades, the extended Derjaguin-Landau-Verwey-Overbeek (XDLVO) theory has been applied as both qualitative and quantitative models to predict and explain bacterial adhesion to surfaces [4,25,53]. In this theory, bacterial adhesion results from a combination of distance-dependent interactions including Lifshitz-Van der Waals (LW) forces, electrostatic double-layer (EL) interactions, acid-base binding (AB) and Brownian motion (Br). Compared to the classic DLVO theory, the short-range AB interactions describe attractive hydrophobic attractions or repulsive hydrophilic repulsions or hydration effects which may be 10–100 times stronger than LW and EL interactions [25,54].

In this study, the total interaction energy ΔE^{TOT} as a function of separation distance (H) was calculated according to our previous studies using both DLVO and XDLVO models [26,33]. The contact angles and surface energy data are shown in Table 1. As seen in Fig. 2d, the ΔE^{TOT} curve demonstrated a very clear secondary minimum of about $-3.9E^{-20}$ J (-10 kT) at about 7 nm and an energy barrier of up to 1.2 E^{-17} J (290 kT) at 0.157 nm from the 316L SS surface. Comparing the classic DLVO and XDLVO models, the acid-base (AB) interactions only affected the energy curve at close separation distances within the primary minimum but not at the secondary minimum. In contrast to the hydrophilic 316L SS surface, the LW reactions at the hydrophobic PTFE surfaces were repulsive and bacterial adhesion should not occur according to the classical DLVO theory (Fig. 2e). However, the XDLVO model predicted very strong interaction due to the acid-base interactions leading to an extremely deep minimum at 0.157 nm (primary minimum) at which bacterial cells are considered to be irreversibly attached to surfaces. Fig. 2f shows the influence of minimum interaction energy (ΔE_{min}^{TOT}) on biomass formation over contact time. It seems that the biofilm was less prone to accumulate on the surface with higher ΔE_{min}^{TOT}, which is consistent with the XDLVO theory.

3.4. Corrosion resistance

Corrosion resistance is an essential characteristic of metallic implants for clinical applications. However, 316L SS surfaces in physiological solutions are often subjected to localized corrosion such as pitting and crevice formation, which may induce mechanical failure and severe complications [55,56,2]. In this study, the corrosion resistance of 316L SS, PTFE and AP coatings was studied *via* an electrochemical method in PBS. Fig. 4a presents the OCP (E_{oc}) curves of the coated and uncoated surfaces during the initial 3600 s. The corrosion potentials of both PTFE and AP coated samples shifted towards a nobler direction indicating an improved anodic protection for the 316L SS substrate in PBS. A passivation layer was formed on the 316L SS surface which resulted in a rapid increase in the OCP (E_{oc}) in the initial 1000 s [57]. In comparison, the OCPs of PTFE coated samples remained at a relatively stable level during the whole test period. Notably, the AP coatings (-138 mV for AP-1 and -173 mV for AP-2) presented more negative OCPs compared with the PTFE coating (-68 mV) and the corrosion potentials slightly decayed over time. As the AgNP deposition process is slowly reversible, the decrease in OCP (E_{oc}) may be caused by the oxidation of AgNPs in the presence of PBS [58]. Fig. 4b shows the polarization curves of the uncoated and coated samples. The corrosion

Table 1
Contact angle and surface energy data (n = 6, bars are standard error of the mean).

Samples	Contact angle, θ (deg)			Surface free energy (mJ/m^2)			
	θ^W	θ^D	θ^E	γ^{LW}	γ^+	γ^-	γ^{TOT}
316L SS	69.2 ± 0.7	38.4 ± 0.3	47.2 ± 0.9	40.41	0.02	14.18	41.35
PTFE	105.5 ± 1.4	75.4 ± 1.1	79.0 ± 0.8	19.91	0.29	0.38	20.58
AP-1	108.0 ± 0.8	69.6 ± 0.3	84.5 ± 1.2	23.10	0.00	0.22	23.15
AP-2	112.1 ± 1.3	78.2 ± 0.6	90.3 ± 0.4	18.43	0.00	0.29	18.43
E. coli, WT F1693 [38]	16.5 ± 1.1	47.6 ± 0.5	22.9 ± 0.7	35.60	0.14	67.68	41.76

potentials (E_{corr}) and the corrosion current densities (i_{corr}) were derived directly from the polarization curves by the Tafel extrapolation method. As demonstrated in Fig. 4c, all the coatings exhibited more positive E_{corr} and dramatically lower i_{corr} than the uncoated substrate. The PTFE coating exhibited the best substrate protection as the i_{corr} parameter was over one order of magnitude lower in value than the 316L SS substrate. After AgNP deposition, the corrosion resistance was slightly compromised and a longer deposition time resulted in a decrease in the value of E_{corr}. However, the I_{corr} values of the AP coatings (1.58×10^{-7} A/cm^2 for the AP-1 and 2.51×10^{-7} A/cm^2 for the AP-2) were still about one magnitude lower than the substrate (2.01×10^{-6} A/cm^2), indicating an enhanced corrosion protection.

3.5. Cytotoxicity assay

In this study, the cytotoxicity of the coatings was examined using a direct contact method with L929 mouse fibroblasts for up to 72 h considering the initial burst release of Ag^+ from the AP coatings (Fig. 2a). As demonstrated in Fig. 5, the uncoated 316 L SS and PTFE coated samples exhibited the lowest cytotoxicity during 72 h of culturing and no significant difference was found in the OD values between these two groups ($p > 0.05$). The presence of AgNP significantly

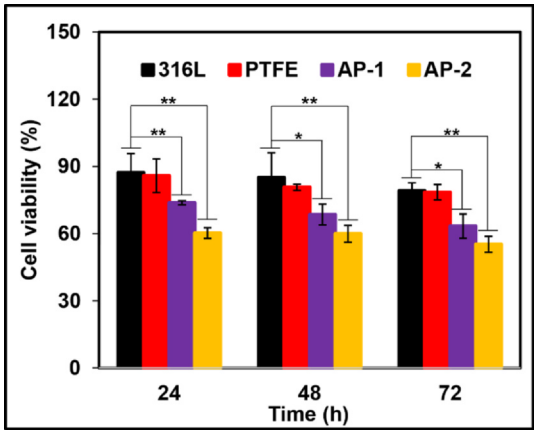

Fig. 5. MTT assay for the viability of L929 cells cultured with 316L SS, PTFE, AP-1 and AP-2 at 24, 48 and 72 h. (* $p < 0.05$ and ** $p < 0.01$ compared with control).

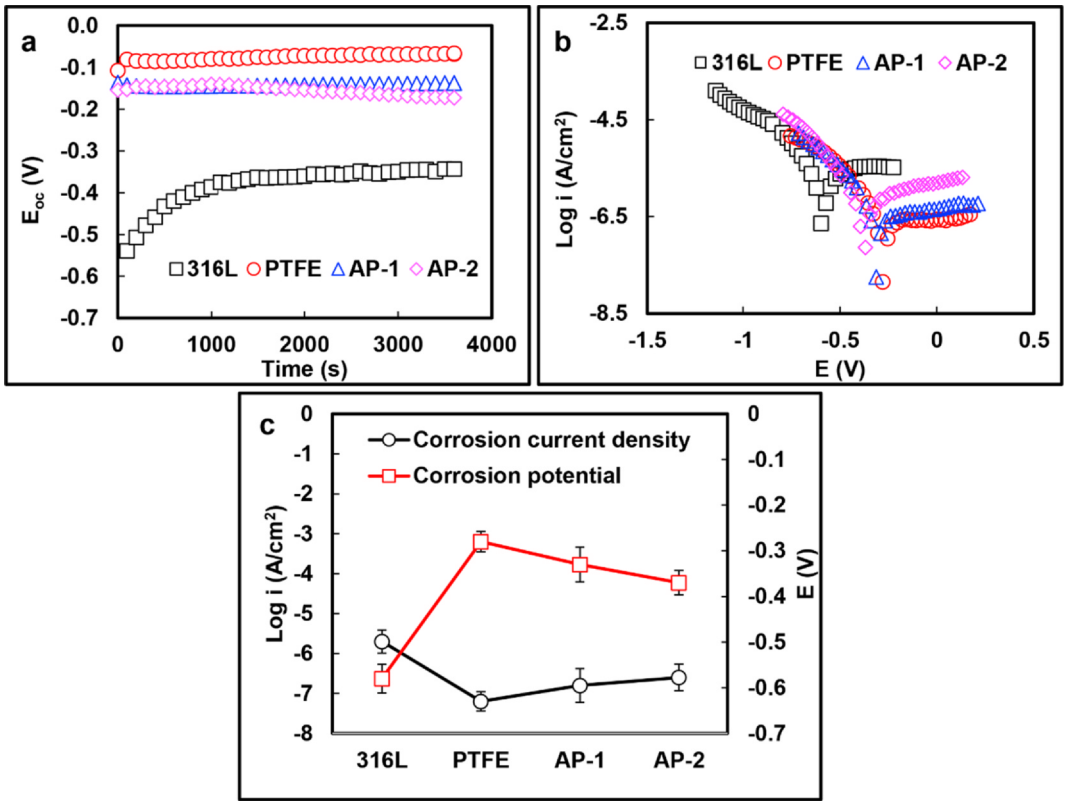

Fig. 4. (a) Open-circuit potential, (b) potentiodynamic polarization curves and (c) the E_{corr} and Log i_{corr} of different samples in PBS (n = 3, bars represent standard deviation of the mean).

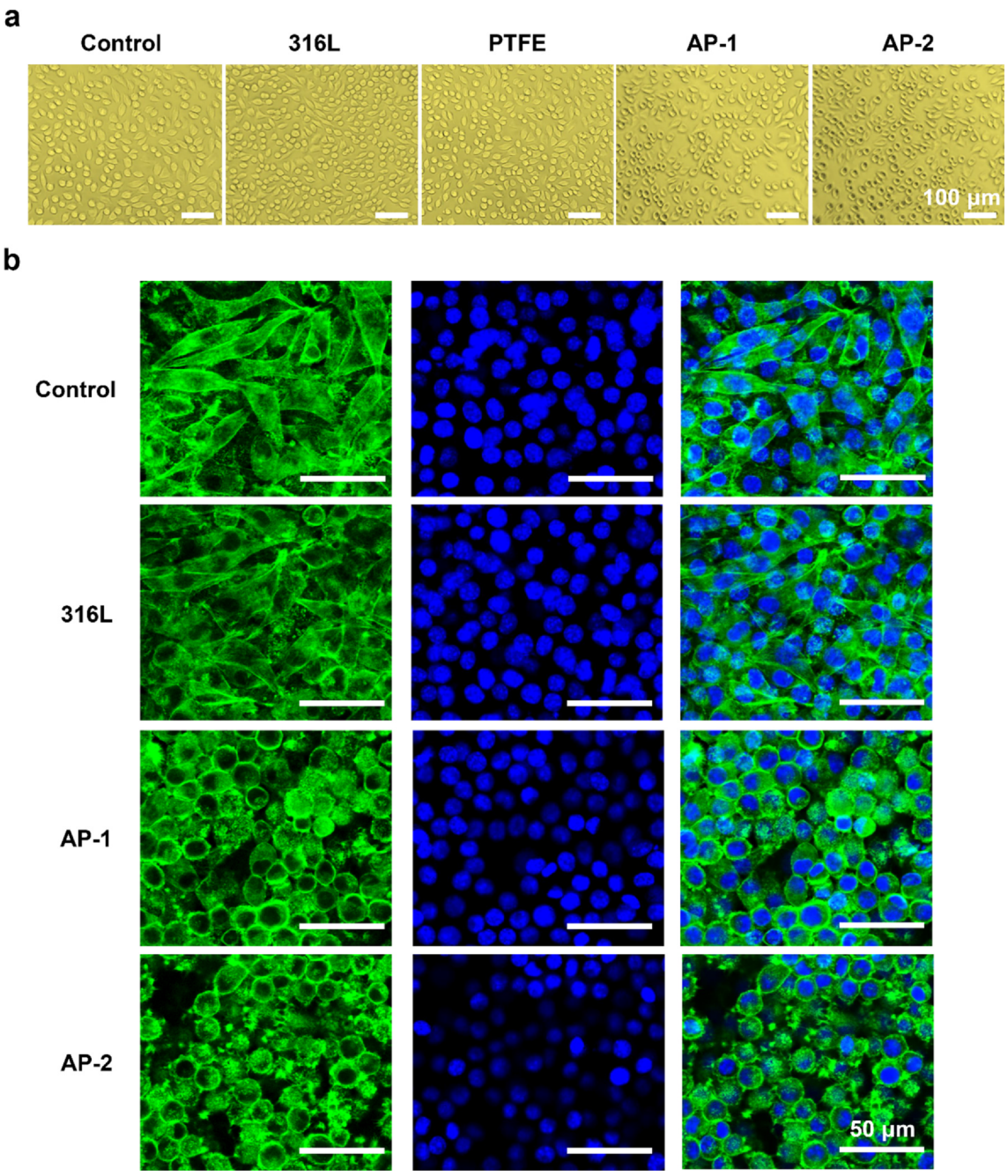

Fig. 6. (a) Optical images of L929 cells after 24 h of co-incubation and (b) confocal microscopy images of L929 cells after 72 h of co-incubation (the nuclei were stained with Hoechst 33258, the actin cytoskeleton was labeled using Alexa Fluor 488 phalloidin). Typical images are shown from one of several examinations.

inhibited the proliferation of L929 cells as the medium with AP coatings showed the lowest OD value over the whole test period. Moreover, it is noteworthy that the adverse effects of AP coatings were Ag^+-concentration-dependent. Following 24 h incubation, the AP-1 and AP-2 coatings inhibited bacterial growth by 26.3% and 39.7% respectively when compared with the control. After 72 h, the inhibition rates rosed to 36.7% (AP-1) and 44.8% (AP-2), respectively. According to the ISO 10993–5:2009(E), the samples would be considered to have cytotoxic effects if the cell viability was reduced to < 70% of the blank. Therefore, the results indicated that the AP coatings would result in a toxic effect towards the L929 cells after 72 h culture despite AP-1 demonstrated being biocompatible over the first 24 h. This may be caused by the accumulation of silver ions in the culture medium that induced a toxic response over time. According to previous studies [59], the commercial silver coated urinary catheter (Dover™) only released ~0.30 μg/cm^2 of Ag per day in the initial 3 days while the amount of Ag released from AP coatings was 3–4 times higher (Table S1).

Cell morphologies were observed using both optical and confocal microscopy. As seen in Fig. 6, after 24 h culturing, L929 cells in the control wells exhibited a healthy and heterogeneous profile, including spindle-like, stellate and round shapes. Cells cultivated in the medium which was initially incubated with 316L SS and PTFE coated samples showed a similar morphology to control cells. However, it was found that some of the cells exposed to the AP coatings lost their typical spindle-shaped morphology and features such as shrinkage, cytoplasmic condensation and rounded cells were observed in the AP-2 group. After 72 h, the cells exposed to AP coatings had almost lost their elongated shape, and the majority had an oval or rounded shape. Similar results have been reported in other studies [60,61].

4. Conclusions

In this paper, a sol–gel derived AP coating was fabricated for metallic implants *via* a facile layer-by layer method. A mussel-inspired PDA layer was first applied onto the substrate to encourage the immobilization of the sol–gel matrix which provided a platform for the subsequent entrapment of PTFE and deposition of AgNP. Benefiting from their synergistic effect, the AP coating exhibited prolonged antibacterial activity against *E. coli* and enhanced corrosion resistance in PBS. The AP coating was capable of releasing antibacterial Ag^+ in a sustained manner which was proved to effectively inhibit bacterial growth and retard biofilm formation. Despite concerns that overdose of Ag^+ could cause local cytotoxicity, the coating procedures offered an ease of control over the silver release and demonstrated good practicability, making it potentially useful in preventing the metallic implant-associated infections.

CRediT authorship contribution statement

Shuai Zhang: Conceptualization, Methodology, Investigation, Writing - original draft. **Xinjin Liang:** Investigation, Methodology, Formal analysis, Writing - original draft. **Geoffrey Michael Gadd:** Investigation, Formal analysis, Supervision. **Qi Zhao:** Conceptualization, Methodology, Resources, Supervision, Project administration.

Declaration of Competing Interest

The authors declare that they have no known competing financial interests or personal relationships that could have appeared to influence the work reported in this paper.

Acknowledgements

This work was supported by the UK Engineering and Physical Sciences Research Council (EP/P00301X/1).

Appendix A. Supplementary material

Supplementary data to this article can be found online at https://doi.org/10.1016/j.apsusc.2020.147675.

References

[1] K. Prasad, O. Bazaka, M. Chua, M. Rochford, L. Fedrick, J. Spoor, R. Symes, M. Tieppo, C. Collins, A. Cao, D. Markwell, K.K. Ostrikov, K. Bazaka, Metallic biomaterials: current challenges and opportunities, Materials (Basel, Switzerland) 10 (8) (2017) 884.
[2] Q. Chen, G.A. Thouas, Metallic implant biomaterials, Mater. Sci. Eng. R Rep. 87 (2015) 1–57.
[3] L.H. Stoodley, J.W. Costerton, P. Stoodley, Bacterial biofilms: from the natural environment to infectious diseases, Nat. Rev. Microbiol. 2 (2) (2004) 95–108.
[4] R.M. Donlan, J.W. Costerton, Biofilms: survival mechanisms of clinically relevant microorganisms, Clin. Microbiol. Rev. 15 (2) (2002) 167–193.
[5] J. Song, H. Liu, M. Lei, H. Tan, Z. Chen, A. Antoshin, G.F. Payne, X. Qu, C. Liu, Redox-channeling polydopamine-ferrocene (PDA-Fc) coating to confer context-dependent and photothermal antimicrobial activities, ACS Appl. Mater. Interfaces. 12 (7) (2020) 8915–8928.
[6] D. Mitra, E.T. Kang, K.G. Neoh, Antimicrobial copper-based materials and coatings: potential multifaceted biomedical applications, ACS Appl. Mater. Interfaces. 12 (19) (2020) 21159–21182.
[7] Q. Xue, X.B. Liu, Y.H. Lao, L.P. Wu, D. Wang, Z.Q. Zuo, J.Y. Chen, J. Hou, Y.Y. Bei, X.F. Wu, K.W. Leong, H. Xiang, J. Han, Anti-infective biomaterials with surface-decorated tachyplesin I, Biomaterials 178 (2018) 351–362.
[8] X. Shen, Y. Zhang, P. Ma, L. Sutrisno, Z. Luo, Y. Hu, Y. Yu, B. Tao, C. Li, K. Cai, Fabrication of magnesium/zinc-metal organic framework on titanium implants to inhibit bacterial infection and promote bone regeneration, Biomaterials 212 (2019) 1–16.
[9] E.L. Cyphert, H.A. von Recum, Emerging technologies for long-term antimicrobial device coatings: advantages and limitations, Exp. Biol. Med (Maywood) 242 (8) (2017) 788–798.
[10] Z.K. Zander, M.L. Becker, Antimicrobial and antifouling strategies for polymeric medical devices, ACS Macro. Lett. 7 (1) (2018) 16–25.
[11] Y.K. Jo, J.H. Seo, B.H. Choi, B.J. Kim, H.H. Shin, B.H. Hwang, H.J. Cha, Surface-independent antibacterial coating using silver nanoparticle-generating engineered mussel glue, ACS Appl. Mater. Interfaces. 6 (22) (2014) 20242–20253.
[12] Y.H. Huang, M.H. Chen, B.H. Lee, K.H. Hsieh, Y.K. Tu, J.J. Lin, C.H. Chang, Evenly distributed thin-film Ag coating on stainless plate by tricomponent Ag/silicate/PU with antimicrobial and biocompatible properties, ACS Appl. Mater. Interfaces. 6 (22) (2014) 20324–20333.
[13] S. Zhang, L. Wang, X. Liang, J. Vorstius, R. Keatch, G. Corner, G. Nabi, F. Davidson, G.M. Gadd, Q. Zhao, Enhanced antibacterial and antiadhesive activities of silver-PTFE nanocomposite coating for urinary catheters, ACS Biomater. Sci. Eng. 5 (6) (2019) 2804–2814.
[14] A. Panáček, L. Kvítek, M. Smékalová, R. Večeřová, M. Kolář, M. Röderová, F. Dyčka, M. Šebela, R. Prucek, O. Tomanec, R. Zbořil, Bacterial resistance to silver nanoparticles and how to overcome it, Nat. Nanotechnol. 13 (2018) 65–71.
[15] S.L. Percival, P.G. Bowler, D. Russell, Bacterial resistance to silver in wound care, J. Hosp. Infect. 60 (1) (2005) 1–7.
[16] R.O. Darouiche, Anti-infective efficacy of silver-coated medical prostheses, Clin. Infect. Dis. 29 (6) (1999) 1371–1377.
[17] J.M. Schierholz, L.J. Lucas, A. Rump, G. Pulverer, Efficacy of silver-coated medical devices, J. Hosp. Infect. 40 (4) (1998) 257–262.
[18] R. Pickard, T. Lam, G. MacLennan, K. Starr, M. Kilonzo, G. McPherson, K. Gillies, A. McDonald, K. Walton, B. Buckley, C. Glazener, C. Boachie, J. Burr, J. Norrie, L. Vale, A. Grant, J. N'Dow, Antimicrobial catheters for reduction of symptomatic urinary tract infection in adults requiring short-term catheterisation in hospital: a multicentre randomised controlled trial, Lancet 380 (9857) (2012) 1927–1935.
[19] S. Zhang, X. Liang, G.M. Gadd, Q. Zhao, Superhydrophobic coatings for urinary catheters to delay bacterial biofilm formation and catheter-associated urinary tract infection, ACS Appl. Bio Mater. 3 (1) (2020) 282–291.
[20] S. Mei, H. Wang, W. Wang, L. Tong, H. Pan, C. Ruan, Q. Ma, M. Liu, H. Yang, L. Zhang, Y. Cheng, Y. Zhang, L. Zhao, P.K. Chu, Antibacterial effects and biocompatibility of titanium surfaces with graded silver incorporation in titania nanotubes, Biomaterials 35 (14) (2014) 4255–4265.
[21] J. Wang, J. Li, G. Guo, Q. Wang, J. Tang, Y. Zhao, H. Qin, T. Wahafu, H. Shen, X. Liu, X. Zhang, Silver-nanoparticles-modified biomaterial surface resistant to staphylococcus: new insight into the antimicrobial action of silver, Sci. Rep. 6 (2016) 32699.
[22] S. Taheri, A. Cavallaro, S.N. Christo, L.E. Smith, P. Majewski, M. Barton, J.D. Hayball, K. Vasilev, Substrate independent silver nanoparticle based antibacterial coatings, Biomaterials 35 (16) (2014) 4601–4609.
[23] H. Qian, M. Li, Z. Li, Y. Lou, L. Huang, D. Zhang, D. Xu, C. Du, L. Lu, J. Gao, Mussel-inspired superhydrophobic surfaces with enhanced corrosion resistance and dual-action antibacterial properties, Mater. Sci. Eng. C. Mater. Biol. Appl. 80 (2017) 566–577.
[24] C. Levard, E.M. Hotze, G.V. Lowry, G.E. Brown Jr, Environmental transformations of silver nanoparticles: impact on stability and toxicity, Environ. Sci. Technol. 46 (13) (2012) 6900–6914.
[25] M. Hermansson, The DLVO theory in microbial adhesion, Colloids Surf. B. 14 (1–4) (1999) 105–119.
[26] C. Liu, Q. Zhao, The CQ ratio of surface energy components influences adhesion and removal of fouling bacteria, Biofouling 27 (3) (2011) 275–285.
[27] A. Demling, C. Elter, T. Heidenblut, F.W. Bach, A. Hahn, P.R. Schwestka, M. Stiesch, W. Heuer, Reduction of biofilm on orthodontic brackets with the use of a polytetrafluoroethylene coating, Eur. J. Orthod. 32 (4) (2010) 414–418.
[28] A.K. Epstein, T.S. Wong, R.A. Belisle, E.M. Boggs, J. Aizenberg, Liquid-infused structured surfaces with exceptional anti-biofouling performance, Proc. Nat. Acad. Sci. 109 (33) (2012) 13182–13187.
[29] Q. Zhao, Y. Liu, C. Wang, S. Wang, H. Müller-Steinhagenc, Effect of surface free energy on the adhesion of biofouling and crystalline fouling, Chem. Eng. Sci. 60 (17) (2005) 4858–4865.
[30] S. Jindal, S. Anand, K. Huang, J. Goddard, L. Metzger, J. Amamcharla, Evaluation of modified stainless steel surfaces targeted to reduce biofilm formation by common milk sporeformers, J. Dairy. Sci. 99 (12) (2016) 9502–9513.
[31] M.C. Sportelli, E. Tütüncü, R.A. Picca, M. Valentini, A. Valentini, C. Kranz, B. Mizaikoff, H. Barth, N. Cioffi, Inhibiting P. fluorescens biofilms with fluoropolymer-embedded silver nanoparticles: an in-situ spectroscopic study, Sci. Rep. 7 (2017) 11870.
[32] C. Liu, Q. Zhao, Influence of surface-energy components of Ni-P-TiO_2-PTFE nanocomposite coatings on bacterial adhesion, Langmuir 27 (15) (2011) 9512–9519.
[33] E.L. Lawrence, I.G. Turner, Materials for urinary catheters: a review of their history and development in the UK, Med. Eng. Phys. 27 (6) (2005) 443–453.
[34] G.J. Owens, R.K. Singh, F. Foroutan, M. Alqaysi, C.M. Han, C. Mahapatra, H.W. Kim, Sol-gel based materials for biomedical applications, Prog. Mater. Sci. 77 (2016) 1–79.
[35] M. Altstein, A. Bronshtein, Sol-gel immunoassays and immunoaffinity chromatography, in: J.M. Van Emon (Ed.), Immunoassay and Other Bioanalytical Techniques, CRC Press, Taylor and Francis, New York, 2007, pp. 357–383.
[36] D. Roe, B. Karandikar, N. Bonn-Savage, B. Gibbins, J.B. Roullet, Antimicrobial surface functionalization of plastic catheters by silver nanoparticles, J. Antimicrob. Chemother. 61 (4) (2008) 869–876.
[37] L. Wang, S. Zhang, R. Keatch, G. Corner, G. Nabi, S. Murdoch, F. Davidson, Q. Zhao, In-vitro antibacterial and anti-encrustation performance of silver-polytetrafluoroethylene nanocomposite coated urinary catheters, J. Hosp. Infect. 103 (1) (2019) 55–63.
[38] S. Zhang, X. Liang, G.M. Gadd, Q. Zhao, Advanced titanium dioxide-polytetrafluorethylene (TiO_2-PTFE) nanocomposite coatings on stainless steel surfaces with

antibacterial and anti-corrosion properties, Appl. Surf. Sci. 490 (2019) 231–241.
[39] M. Salomäki, L. Marttila, H. Kivelä, T. Ouvinen, J. Lukkari, Effects of pH and oxidants on the first steps of polydopamine formation: a thermodynamic approach, J. Phys. Chem. B. 122 (24) (2018) 6314–6327.
[40] Y. Cong, T. Xia, M. Zou, Z. Li, B. Peng, D. Guo, Z. Deng, Mussel-inspired polydopamine coating as a versatile platform for synthesizing polystyrene/Ag nanocomposite particles with enhanced antibacterial activities, J. Mater. Chem. B 2 (22) (2014) 3450–3461.
[41] C. Wu, G. Zhang, T. Xia, Z. Li, K. Zhao, Z. Deng, D. Guo, B. Peng, Bioinspired synthesis of polydopamine/Ag nanocomposite particles with antibacterial activities, Mater. Sci. Eng. C 55 (2015) 155–165.
[42] Z. Deng, B. Shang, B. Peng, Polydopamine based colloidal materials: synthesis and applications, Chem. Rec. 18 (2018) 410–432.
[43] Z. Zhang, J. Zhang, B. Zhang, J. Tang, Mussel-inspired functionalization of graphene for synthesizing Ag-polydopamine-graphenenanosheets as antibacterial materials, Nanoscale 5 (2013) 118–123.
[44] Z. Wang, J. Li, F. Tang, J. Lin, Z. Jin, Polydopamine nanotubes-templated synthesis of TiO_2 and its photocatalytic performance under visible light, RSC Adv. 7 (2017) 23535–23542.
[45] Y. Zhang, W. Wang, X. Ma, L. Jia, Polydopamine assisted fabrication of titanium oxide nanoparticles modified column for proteins separation by capillary electrochromatography, Anal. Biochem. 512 (2016) 103–109.
[46] Q. Zhao, Y. Liu, S. Wang, Surface modification of water treatment equipment for reducing $CaSO_4$ scale formation, Desalination 180 (1–3) (2005) 133–138.
[47] R. Sieh, H. Le, Non-cyanide electrodeposited Ag-PTFE composite coating using direct or pulsed current deposition, Coatings 6 (3) (2016) 31.
[48] Y. Liu, Q. Zhao, Effects of surfactants on the PTFE particle sizes in electroless plating Ni-P-PTFE coatings, Trans. Inst. Met. Finish. 81 (5) (2003) 168–171.
[49] P.A. Tran, T.J. Webster, Understanding the wetting properties of nanostructured selenium coatings: the role of nanostructured surface roughness and air-pocket formation, Int. J. Nanomed. 8 (2013) 2001–2009.
[50] A. Kędziora, M. Speruda, E. Krzyżewska, J. Rybka, A. Łukowiak, G. Bugla-Płoskońska, Similarities and differences between silver Ions and silver in nanoforms as antibacterial agents, Int. J. Mol. Sci. 19 (2) (2018) E444.
[51] B.M. Karandikar, B.L. Gibbins, K.A. Cornell, Antimicrobial silver compositions, U.S. Patent US8900624B2, January 23, 2019.
[52] B. Molleman, T. Hiemstra, Time, pH, and size dependency of silver nanoparticle dissolution: the road to equilibrium, Environ. Sci. Nano. 4 (6) (2017) 1314–1327.
[53] K. Hori, S. Matsumoto, Bacterial adhesion: From mechanism to control, Biochem. Eng. J. 48 (3) (2010) 424–434.
[54] S. Bayoudh, A. Othmane, L. Mora, H.B. Ouada, Assessing bacterial adhesion using DLVO and XDLVO theories and the jet impingement technique, Colloids. Surf B. Biointerfaces. 73 (1) (2009) 1–9.
[55] Y. Jang, W.T. Choi, C.T. Johnson, A.J. García, P.M. Singh, V. Breedveld, D.W. Hess, J.A. Champion, Inhibition of bacterial adhesion on nanotextured stainless steel 316L by electrochemical etching, ACS Biomater. Sci. Eng. 4 (1) (2018) 90–97.
[56] N. Eliaz, Corrosion of metallic biomaterials: a review, Materials (Basel, Switzerland) 12 (3) (2019) 407.
[57] S. Hiromoto, T. Hanawa, Electrochemical properties of 316L stainless steel with culturing L929 fibroblasts, J. R. Soc. Interface 3 (9) (2006) 495–505.
[58] P.G. Figueiredo, L. Grob, P. Rinklin, K.J. Krause, B. Wolfrum, On-chip stochastic detection of silver nanoparticles without a reference electrode, ACS Sens. 3 (1) (2018) 93–98.
[59] R. Wang, K.G. Neoh, E.T. Kang, P.A. Tambyah, E. Chiong, Antifouling coating with controllable and sustained silver release for long-term inhibition of infection and encrustation in urinary catheters, J. Biomed. Mater. Res. B. Appl. Biomater. 103 (3) (2015) 519–528.
[60] Y.G. Yuan, S. Zhang, J.Y. Hwang, I.K. Kong, Silver nanoparticles potentiates cytotoxicity and apoptotic potential of camptothecin in human cervical cancer cells, Oxid. Med. Cell. Longev. 2018 (2018) 6121328.
[61] L.C. Stoehr, E. Gonzalez, A. Stampfl, E. Casals, A. Duschl, V. Puntes, G.J. Oostingh, Shape matters: effects of silver nanospheres and wires on human alveolar epithelial cells, Part. Fibre. Toxicol. 8 (2011) 36.